Kinetically controlled crystal growth approach to enhance triplet energy migration-based photon upconversion

Taku Ogawa
Nobuhiro Yanai
Hironori Kouno
Nobuo Kimizuka

Kinetically controlled crystal growth approach to enhance triplet energy migration-based photon upconversion

Taku Ogawa,[a] Nobuhiro Yanai,[a,b,]* Hironori Kouno,[a] and Nobuo Kimizuka[a,]*

[a]Kyushu University, Graduate School of Engineering, Center for Molecular Systems, Department of Chemistry and Biochemistry, Nishi-ku, Fukuoka, Japan
[b]PRESTO, JST, Kawaguchi, Saitama, Japan

Abstract. Improving efficiency of triplet–triplet annihilation-based photon upconversion (TTA-UC) in crystalline media is challenging because it usually suffers from the severe aggregation of the donor (sensitizer) molecules in acceptor (emitter) crystals. We show a kinetically controlled crystal growth approach to improve donor dispersibility in acceptor crystals. As the donor–acceptor combination, a benchmark pair of platinum(II) octaethylporphyrin (PtOEP) and 9,10-diphenylanthracene (DPA) is employed. A surfactant-assisted reprecipitation technique is employed, where the concentration of the injected PtOEP–DPA solution holds the key to control dispersibility; at a higher PtOEP–DPA concentration, a rapid crystal growth results in better dispersibility of PtOEP molecules in DPA crystals. The improvement of donor dispersibility significantly enhances the TTA-UC quantum yield. Thus, the inherent function of donor-doped acceptor crystals can be maximized by controlling the crystallization kinetics. © *The Authors. Published by SPIE under a Creative Commons Attribution 3.0 Unported License. Distribution or reproduction of this work in whole or in part requires full attribution of the original publication, including its DOI.* [DOI: 10.1117/1.JPE.8.022003]

1 Introduction

Photon upconversion based on triplet–triplet annihilation (TTA-UC) has attracted much attention for its potential applications in renewable energy production technologies.[1–10] In the typical TTA-UC process, (1) a triplet excited state of the donor is formed by intersystem crossing (ISC) from a photoexcited singlet state, (2) acceptor triplet excited states are populated by triplet energy transfer (TET) from the donor triplets, and (3) annihilation between two acceptor triplets (TTA) generates an acceptor singlet excited state, from which upconverted delayed fluorescence is emitted [Fig. 1(a)]. One of the advantages of TTA-UC is its occurrence at lower excitation intensity compared with the other UC mechanisms due to the large absorption coefficient of the donor chromophores and the long triplet lifetime of acceptor molecules.

To achieve efficient TTA-UC under weak incident light sources, diffusion of triplet species should be high enough to enable annihilation within their lifetimes. Consequently, the majority of TTA-UC systems have been studied in solution[8,11–15] or soft polymer matrices,[16–20] in which the TET and TTA processes are mediated by molecular diffusion and collision. Meanwhile, it is desirable for device applications that TTA-UC processes occur in the solid state without molecular diffusion. In this perspective, it is natural to develop triplet energy migration-based photon upconversion (TEM-UC),[10] in which triplet excitons effectively diffuse in densely organized molecular assemblies without molecular diffusion.[21–32] Among various assembly systems, molecular crystals with ordered chromophore arrangements should be promising for achieving

---

*Address all correspondence to: Nobuhiro Yanai, E-mail: yanai@mail.cstm.kyushu-u.ac.jp; Nobuo Kimizuka, E-mail: n-kimi@mail.cstm.kyushu-u.ac.jp
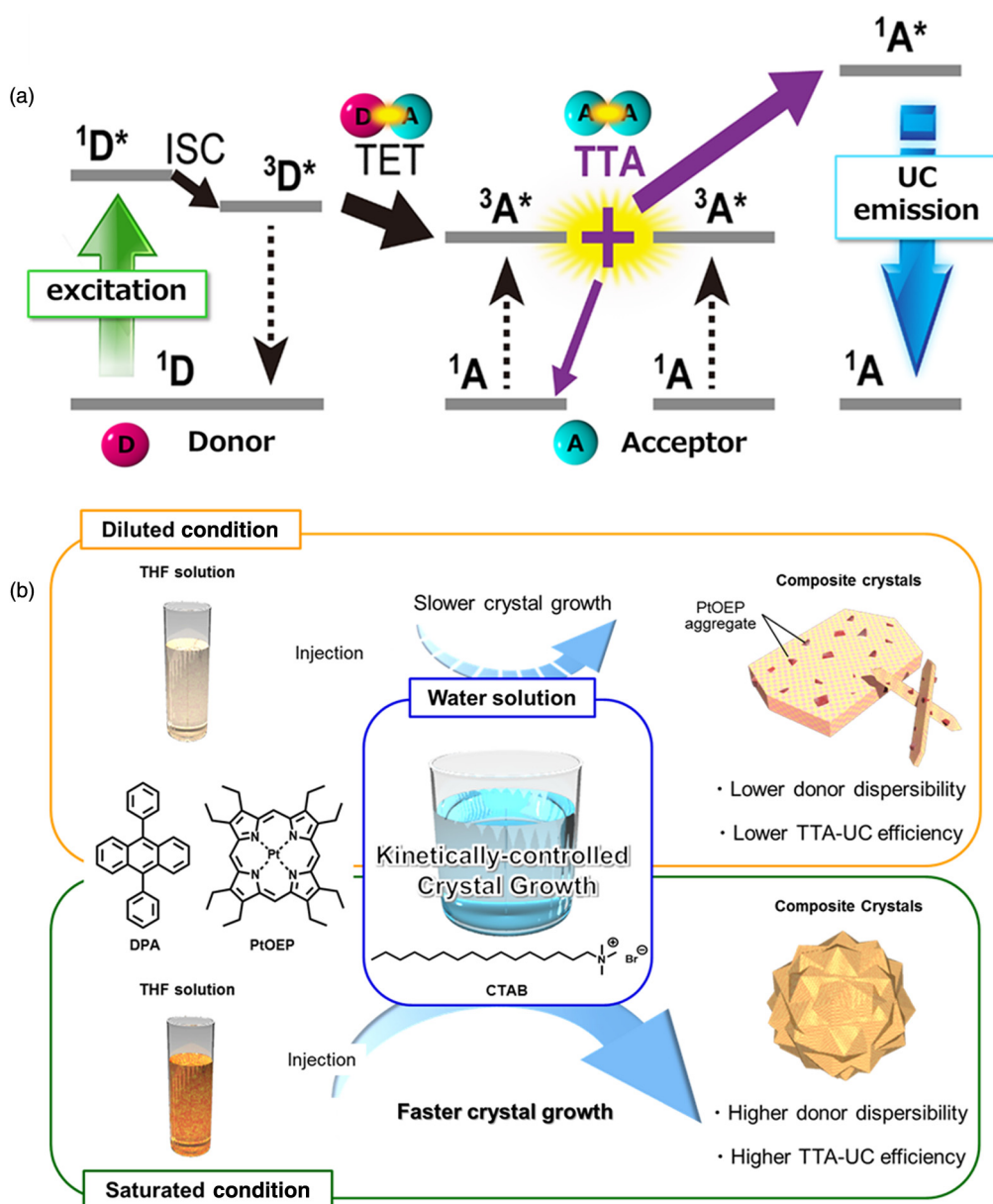
Fig. 1 (a) Typical TTA-UC process with the involved energy levels. (b) Schematic illustration of the concept of this study. DPA–PtOEP composite crystals are formed by reprecipitation in the presence of CTAB. A diluted THF solution of DPA–PtOEP provides slower crystal growth, resulting in lower donor dispersibility and lower TTA-UC efficiency. On the other hand, a saturated THF solution of DPA–PtOEP induces a faster crystal growth, resulting in higher donor dispersibility and higher TTA-UC efficiency.

fast TEM. However, the crystalline systems have suffered from the aggregation of donor molecules and their segregation in acceptor crystals, which caused poor TET efficiency.[4] Despite efforts to solve this problem,[28,29,32–34] the development of a simple and rational strategy to molecularly accommodate donor molecules in acceptor crystals is still anticipated.

Here, we describe a kinetically controlled crystal growth approach that improves the dispersibility of donors in acceptor crystals and, consequently, increased the efficiency of TEM-UC. We employed the donor–acceptor pair of Pt(II) octaethylporphyrin (PtOEP) and 9,10-diphenylanthracene (DPA), which has been widely used as a benchmark. Due to their inherent structural mismatch, PtOEP and DPA do not mix homogeneously in crystals and tend to phase segregate.[4] Meanwhile, miscibility of molecules coexisting in multicomponent

assemblies has been kinetically controlled for organic molecular crystals[35] and peptide assemblies.[36,37] We apply this kinetic control concept to improve the miscibility of donor PtOEP and acceptor DPA in nanocrystals. For this, we adopted a colloid chemistry approach; tetrahydrofuran (THF) solutions of DPA–PtOEP were injected into aqueous cetyltrimethylammonium bromide (CTAB).[38–40] Upon the diffusion of injected THF into the aqueous phase, the nucleation of water-insoluble aromatic crystals occurs. Adsorption of CTAB molecules on the growing crystal surfaces would reduce their interfacial energy, thus enhancing the dispersion stability of these crystals.[38–40] Significantly, it was found that the increase in the concentration of DPA–PtOEP caused faster crystallization of DPA, which allowed PtOEP molecules to be kinetically trapped with improved dispersibility in DPA crystals [Fig. 1(b)].

2 Experimental Details

2.1 *Materials and Methods*

All the solvents were used as received without further purification. DPA was purchased from Aldrich and purified by sublimation in order to minimize the amount of impurities, which may act as quencher in the solid system. PtOEP and CTAB were purchased from Aldrich and Wako chemical and used as received.

UV–visible absorption spectra were recorded on a JASCO V-670 spectrophotometer. Fluorescence spectra were measured by using a PerkinElmer LS 55 fluorescence spectrometer. Powder x-ray diffraction (PXRD) analyses were conducted on a BRUKER D2 PHASER with a Cu Kα source ($\lambda_{ex} = 1.5418$ Å). Scanning electron microscope (SEM) images were obtained by using a Hitachi S-5000. For SEM measurements, samples were collected by suction filtration using membrane filters with pore size of 0.2 μm. These filters were directly used for SEM measurements after platinum sputtering with the thickness of ca. 2 nm. Time-resolved photoluminescence lifetime measurements were carried out by using a time-correlated single photon counting lifetime spectroscopy system, Hamamatsu Quantaurus-Tau C11567-01. Dynamic light scattering measurements were carried out by using Malvern Nano-ZS ZEN3600.

For TTA-UC measurements, the samples were sealed between quartz plates by using hot-melt adhesive in an Ar-filled glove box ($[O_2] < 0.1$ ppm). For TTA-UC emission spectra, a diode laser (532 nm, 200 mW, RGB Photonics) was used as an excitation source. The laser power was controlled by combining a software (Ltune) and a variable neutral density filter and measured using a PD300-UV photodiode sensor (OPHIR Photonics). The laser beam was focused on a sample using a lens. The diameter of the laser beam ($1/e^2$) was measured at the sample position using a CCD beam profiler SP620 (OPHIR Photonics). The typical area of laser irradiation spot estimated from the diameter was 2.9×10^{-4} cm^2. The emitted light was collimated by an achromatic lens, the excitation light was removed using a notch filter (532 nm), and the emitted light was again focused by an achromatic lens to an optical fiber connected to a multichannel detector MCPD-9800, which was supplied and calibrated by Otsuka Electronics and equipped with a CCD sensor for the detection of whole visible range with high sensitivity.

TTA-UC and donor phosphorescence quantum yields were measured by using an absolute quantum yield measurement system. The sample was held in an integration sphere and excited by the laser excitation source (532 nm, 200 mW, RGB Photonics). The scattered excitation light was removed using a 532 nm notch filter, and emitted light was monitored with a multichannel detector C10027-01 (Hamamatsu Photonics). The spectrometer was calibrated including the integration sphere and notch filter by Hamamatsu Photonics.[22]

2.2 *Sample Preparations*

DPA and PtOEP were dissolved in THF at three different concentrations. As a moderately diluted condition, DPA (2 mM)–PtOEP(2 μM) in THF was employed (condition 1). Separately, saturated solutions of DPA (140 mM) with two different PtOEP concentrations (140 and 14 μM) were prepared for the rapid crystallization (conditions 2A and 2B). All the experiments of crystal growth and collection were carried out at room temperature (around

20°C). No preformed crystals in the 140 mM DPA solution were detected from dynamic light scattering measurements. 0.5 mL of DPA–PtOEP mixed THF solutions were rapidly injected into the aqueous CTAB (0.5 mM, 5 mL) at room temperature under 1000 rpm stirring. These mixtures were kept stirring for 3 min and then left to stand for 2 h. After the incubation for 2 h, the crystals were collected by centrifugation at 10,000 rpm for 5 min, washed with water for three times, and dried under vacuum at room temperature.

3 Results and Discussions

3.1 Characterization of the Crystals

When the THF solution of DPA (2 mM)–PtOEP (2 μM) was injected into the aqueous CTAB (condition 1) under stirring, the immediately formed suspension turned into a uniform dispersion within 3 min of stirring. This specimen was then incubated for 2 h, during which crystalline particles were gradually formed. On the other hand, precipitates were immediately formed upon injection of the saturated DPA solutions into aqueous CTAB ([DPA] = 140 mM, [PtOEP] = 140 and 14 μM, conditions 2A and 2B), which showed almost no changes during the standing for 2 h.

The composition of the obtained crystals was determined by dissolving the crystals in THF and measuring their absorption spectra. The DPA–PtOEP molar ratios were 2100:1, 700:1, and 7300:1 for those obtained under the conditions 1, 2A, and 2B, respectively. The content of PtOEP in the obtained crystals was lower than the initial mixing ratio in THF for condition 1 (1000:1), whereas it was higher than those for conditions 2A (1000:1) and 2B (10, 000:1). The enhanced accumulation of PtOEP in DPA crystals under conditions 2A and 2B suggests that the rapid growth of DPA microcrystals facilitate kinetic entrapment of PtOEP molecules in the interior.

The crystallinity of obtained samples was confirmed by using PXRD measurements (Fig. 2). The diffraction patterns of the crystals formed under these conditions showed good agreements with the PXRD pattern of bulk DPA. On the other hand, the diffraction peaks of bulk PtOEP, for example, the peak at $2\theta = 9.5$ deg, were hardly observed from those of the composite crystals, which would be due to the high dispersibility of the donor molecules or the too small amount of PtOEP for detection. It is confirmed that the basic arrangement of DPA molecules is almost independent of the crystallization conditions.
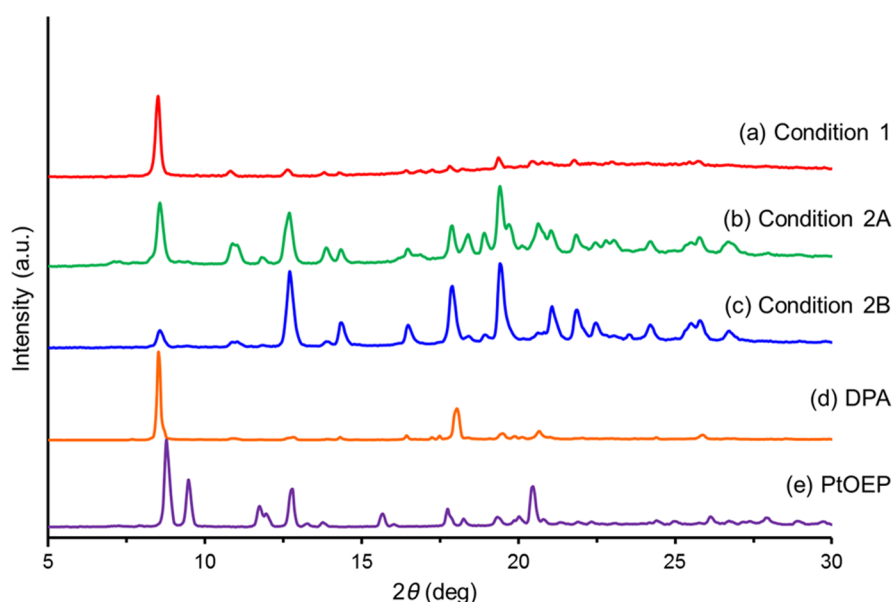
Fig. 2 PXRD patterns of samples prepared by using (a) condition 1, (b) condition 2A, and (c) condition 2B. PXRD patterns of (d) bulk DPA and (e) bulk PtOEP.
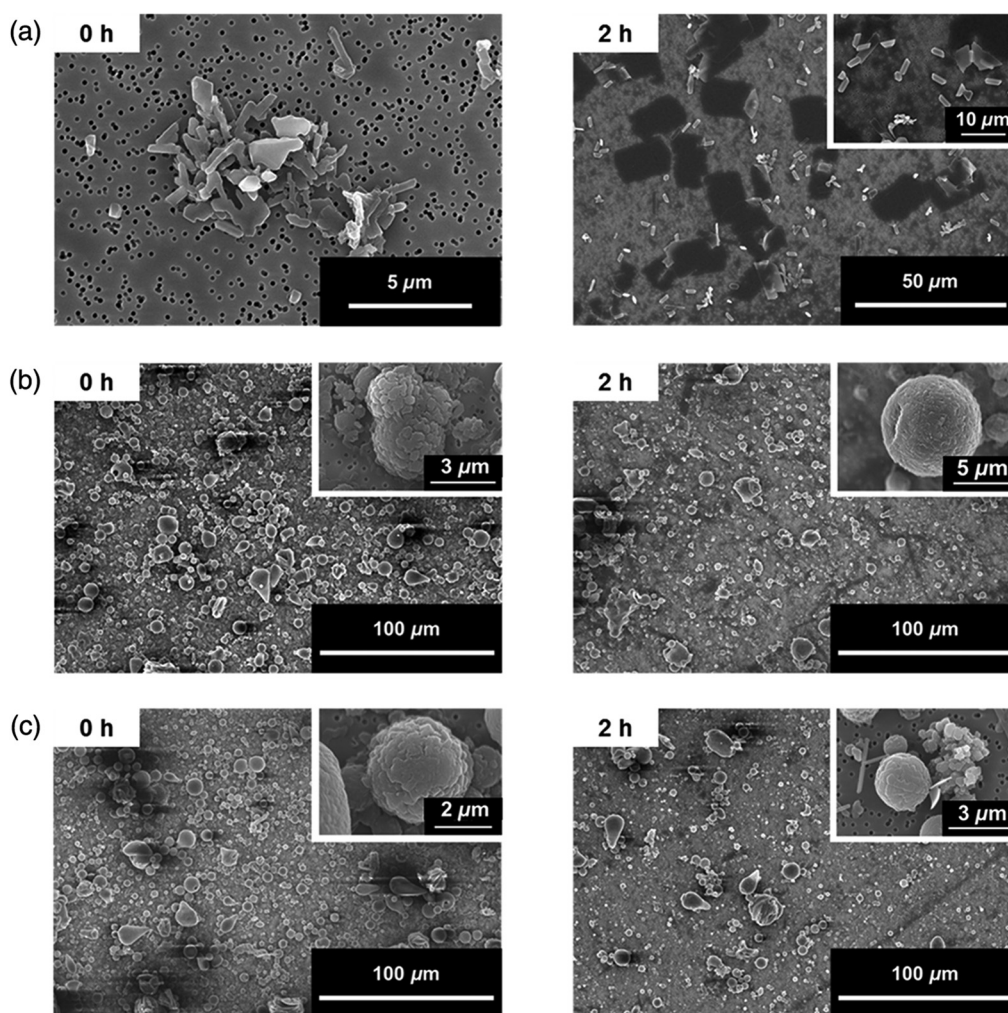
Fig. 3 SEM images of crystals prepared by using (a) condition 1, (b) condition 2A, and (c) condition 2B (left) before and (right) after 2-h incubation.

To get insights into the crystal growth processes, the crystals were collected by suction filtration before and after the 2 h of incubation, and their morphology was observed by scanning electron microscopy. In the case of the condition 1 sample, partly aggregated irregular nanorods were observed before incubation. After standing for 2 h, a few μm-sized rods and a few tens of μm-sized sheets appeared [Fig. 3(a)]. The observed morphological changes suggest that the ordered crystals gradually grew in the course of incubation. On the other hand, samples obtained under the conditions 2A and 2B gave larger spherical microstructures with similar size before and after the incubation process [Figs. 3(b) and 3(c)]. It is to be noted that the morphology of crystals differs considerably depending on the preparative conditions, i.e., kinetic parameters determine both of the nucleation and growth processes. When the same preparation procedure was carried out for PtOEP without DPA, only a few tens of nm-sized nanocrystals were observed, and thus the above-mentioned μm-sized objects cannot be the crystals consisting of pure PtOEP.

3.2 Photophysical Properties of the Crystals

To investigate the dispersed state of PtOEP molecules in acceptor DPA crystals, UV–vis absorption spectra of PtOEP were measured (Fig. 4). A THF solution of PtOEP ([PtOEP] = 10 μM) showed a $Q(0,0)$ band at 534 nm, whereas this band is red-shifted to 552 nm in the cast solid sample due to aggregation.[41] Interestingly, absorption spectra obtained for PtOEP in
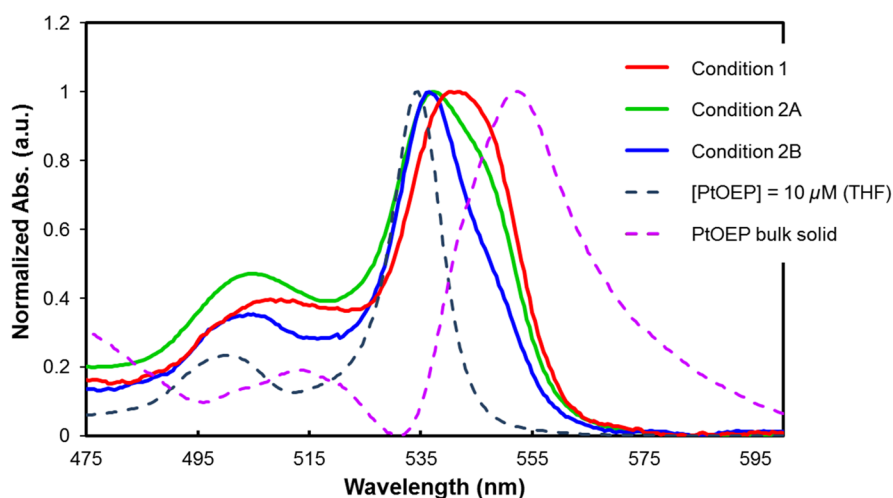
Fig. 4 UV–vis absorption spectra of PtOEP in several conditions. Solid lines represent the absorption of the DPA–PtOEP composite crystals. Dashed lines show the absorption spectra of a diluted THF solution of PtOEP (10 μM) and a bulk PtOEP solid.

DPA–PtOEP composite crystals showed blue shifts compared to that of the neat cast solid. Notably, the peaks of the condition 2A (537 nm) and 2B (536 nm) samples are more blue shifted compared to that of the crystals obtained under condition 1 (541 nm). It is to note that the main peak of the condition 2B sample is close to that observed for the diluted THF solution, with a suppressed shoulder component at around 547 nm. This shoulder component reflects the presence of interchromophore interactions among PtOEP molecules. Apparently, the sample prepared under the condition 2B showed the spectrum revealing the most isolated PtOEP chromophores, showing the highest dispersibility of PtOEP is achieved under the rapid crystal growth condition with the high DPA:PtOEP molar ratio. We confirmed that the DPA–PtOEP crystals prepared in the absence of CTAB showed a pronounced aggregate-shoulder peak, indicating that CTAB significantly influenced the crystallization kinetics in the aqueous mixtures.

The fluorescence quantum yields with direct excitation of DPA (Φ_A, $\lambda_{ex} = 365$ nm) were 42%, 28%, and 54% for powdery samples obtained under conditions 1, 2A, and 2B, respectively. Since the higher Φ_A values were observed for crystals with lower PtOEP contents, it is possible that the DPA-to-PtOEP singlet–singlet energy transfer and/or the reabsorption of the DPA fluorescence by the donor molecules takes place.

The TTA-UC characteristics of each composite crystals were then evaluated. Under excitation with a 532-nm laser, upconverted emission was clearly observed for each sample with the maximum intensity at around 440 nm (Fig. 5). It is to be noted that these TTA-UC behaviors observed for the present DPA–PtOEP crystals prepared by the CTAB-assisted colloid technique is significantly improved as compared to that previously reported for the DPA single crystal doped with PtOEP.[4]

The donor phosphorescence at 650 nm was much weaker than the UC emission, and the phosphorescence quantum yields of all the three samples were less than 0.1%. These results suggest that the triplet energy of the donor molecules is efficiently transferred to the surrounding acceptor molecules or thermally dissipated in the donor aggregates.[41]

TTA-UC quantum yields for samples obtained under each condition were determined by the absolute method using the integrating sphere and the laser excitation source, to avoid inaccuracy that could arise from the strong light scattering of the crystals. In general, the quantum yield is defined as the ratio of absorbed photons to emitted photons, and thus the maximum yield (Φ_{UC}) of the bimolecular TTA-UC process is 50%. However, many reports multiply this value by 2 to set the maximum quantum yield at 100%. To avoid the confusion between these different definitions, the UC quantum yield is written as Φ'_{UC} ($= 2\Phi_{UC}$) when the maximum efficiency is normalized to 100%. The Φ'_{UC} value determined for the condition 1 sample was as low as 0.044 ± 0.011% (Fig. 6). On the other hand, much higher Φ'_{UC} values were observed for crystals prepared under the conditions 2A (0.44 ± 0.022%) and 2B (2.0 ± 0.17%).
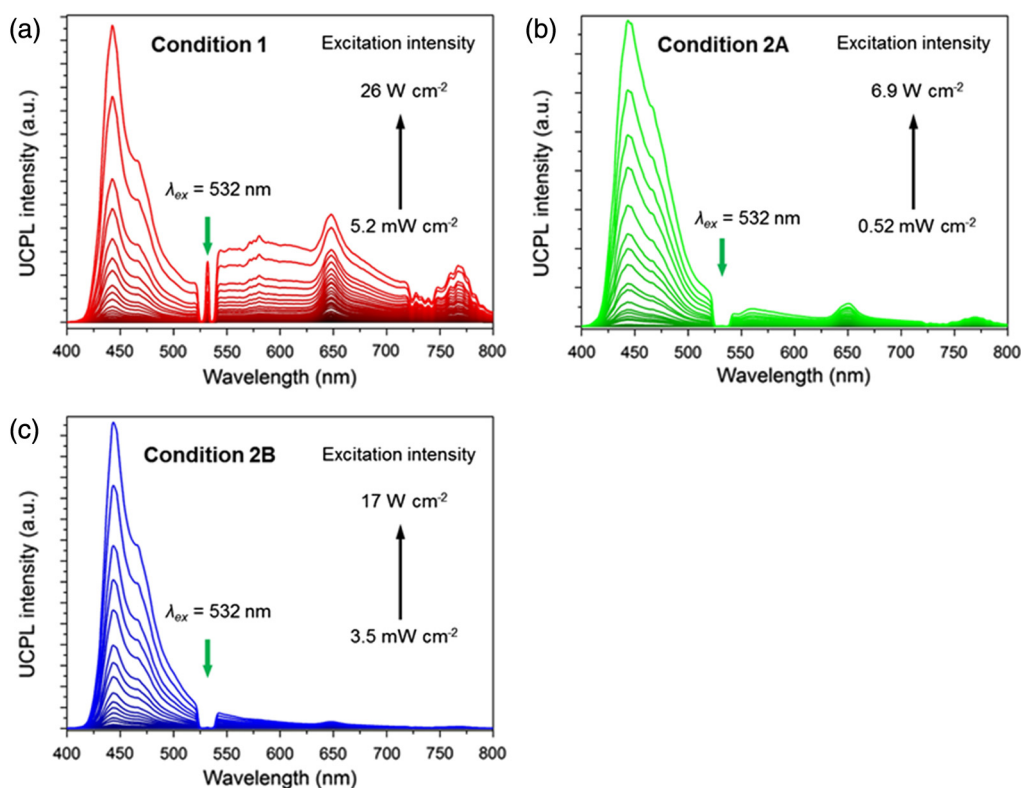
Fig. 5 Photoluminescence spectra of DPA-based crystals prepared under (a) condition 1, (b) condition 2A, and (c) condition 2B under Ar atmosphere with various excitation intensities ($\lambda_{ex} = 532$ nm). Scattered incident light was removed by using a 532 nm notch filter.

To understand the observed difference, factors affecting to the Φ'_{UC} value need to be considered. Φ'_{UC} is represented by the following equation:

$$\Phi'_{UC} = f\Phi_{ISC}\Phi_{ET}\Phi_{TTA}\Phi_A, \tag{1}$$

where Φ_{ISC}, Φ_{ET}, Φ_{TTA}, and Φ_A represent the quantum efficiencies of donor ISC, donor-to-acceptor TET, TTA, and acceptor emission.[4,8] The parameter f is the statistical probability for obtaining a singlet excited state after the annihilation of two triplet states. Considering that Φ_A of the condition 2A sample was smaller (28%) than that of the condition 1 sample (42%), the higher Φ'_{UC} value of the condition 2A sample as compared to the condition 1 sample should be originated from the other parameters. The f value and Φ_{ISC} can be assumed to be the same for the identical donor–acceptor pair with the similar crystal structure as confirmed by PXRD. It is then suggested that the better dispersibility of donor molecules in condition 2A sample, as evidenced by the absorption spectra (Fig. 4), improved the net Φ_{ET} value and consequently afforded the better Φ'_{UC}. As described above, the condition 2B sample showed the highest donor dispersibility among all the samples prepared in this study (Fig. 4). It is reasonable that the condition 2B sample showed higher Φ'_{UC} than the condition 2A sample, which was also benefitted from the smaller content of the donor that allowed to maintain higher Φ_A (54%). The UC quantum yields Φ'_{UC} remain low (<0.1%) at the solar irradiance (1.6 mW cm^{-2} at 532 ± 5 nm, air mass 1.5), requiring future efforts to decrease the needed excitation intensity.

We would like to call attention to the complexity of the condensed systems when the donor distribution is not homogeneous in acceptor crystals. Generally, TTA-UC emission intensity shows a quadratic dependence with the incident light intensity at low excitation intensity, where the thermal deactivation of the triplet states is governed by the main deactivation pathway. The quadratic-to-linear transition occurs by increasing the excitation intensity, and the transition point gives a threshold excitation intensity (I_{th}).[42–44] Above I_{th}, the TTA becomes the main deactivation channel for the acceptor triplets. The quadratic-to-linear transitions were
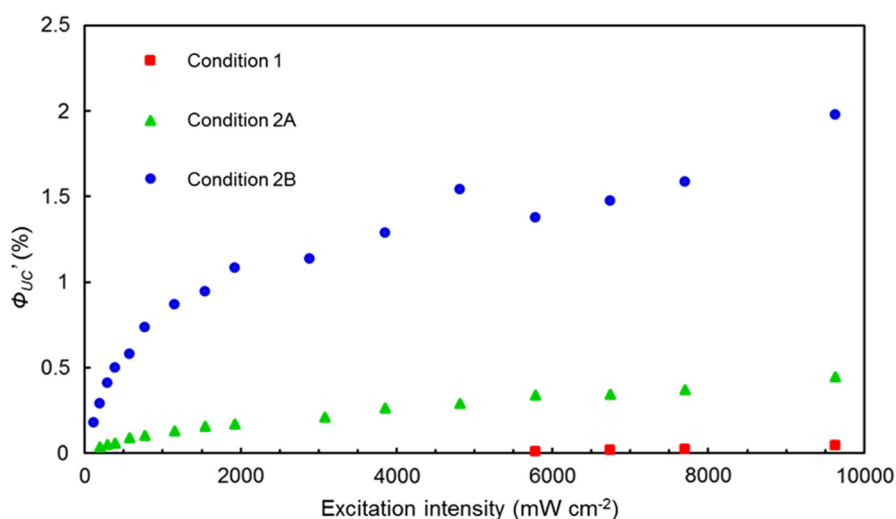
Fig. 6 TTA-UC quantum yield as a function of the excitation intensity of 532-nm laser for DPA–PtOEP composite crystals prepared with three different conditions. A series of Φ'_{UC} data for each sample were obtained from the same specimen, and each points show average values of measurements conducted for more than five times. Error bars are smaller than the dot sizes for most points.

observed for all the three conditions (Fig. 7). Despite the considerable difference in the UC quantum yield (Fig. 6), these three samples showed rather similar I_{th} values in the range of 326 to 531 mW cm^{-2}.

This discrepancy might be explained by the following hypothesis. In the condition 1 sample, not all donor molecules form aggregates and some donor molecules well dispersed in acceptor crystals contribute to the excitation intensity dependence with I_{th} value similar to the condition 2B sample. However, as we described above, most of the donor molecules are present as aggregates in the condition 1 sample, which hinder the donor-to-acceptor TET and resulted in the observed low UC quantum yield. It is therefore essential to characterize the UC characteristics in a comprehensive manner, and the determination of UC quantum yields is prerequisite for the evaluation of solid upconverters.
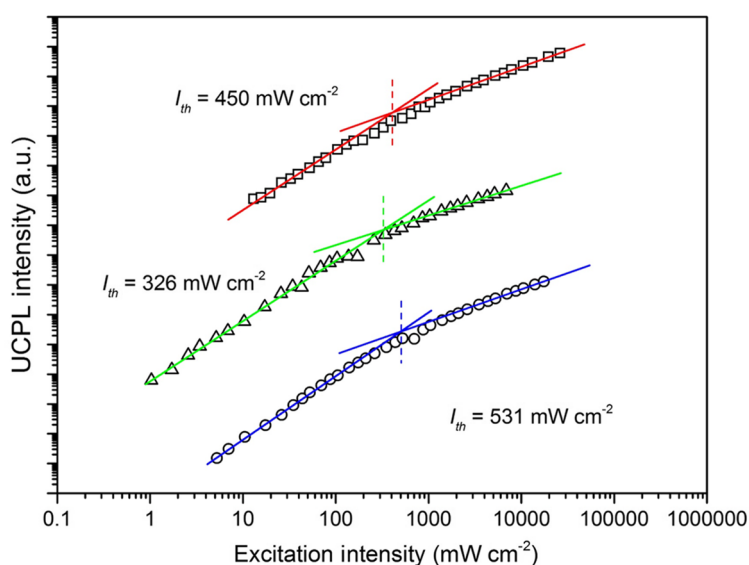
Fig. 7 Double logarithmic plots of the UC photoluminescence intensity as a function of the excitation intensity for DPA–PtOEP composite crystals prepared with three different conditions. The linear fits with slope 2 and 1 in the lower and higher excitation intensity regimes are shown.

4 Conclusions and Future Remarks

We show the promising potential of kinetically controlled crystal growth to improve the dispersibility of donor molecules in acceptor crystals and to achieve efficient TEM-UC in the solid state. By simply increasing the concentration of the donor and acceptor in the surfactant-assisted reprecipitation process, the kinetic entrapment of the donor in acceptor crystals is facilitated with the enhanced dispersibility. Consequently, the UC quantum yield was dramatically enhanced. The concept of kinetically controlled crystal growth is successfully demonstrated for the benchmark TTA-UC pair, DPA and PtOEP, which has been known to undergo severe phase segregation. The present kinetically controlled crystallization concept for improving donor dispersibility in acceptor crystals would be widely applicable to a variety of chromophore combinations, including the recently developed precious metal-free systems[25,45,46] and NIR-to-visible UC systems.[12–15,47,48] For further improvement of the current method, we consider that the key is to suppress the formation of defect sites that deactivate the triplet excitons.[28] The development of approaches to circumvent this issue is under way in our laboratory.

Acknowledgments

References

1. S. Baluschev et al., "Up-conversion fluorescence: noncoherent excitation by sunlight," *Phys. Rev. Lett.* **97**, 143903 (2006).
2. T. N. Singh-Rachford and F. N. Castellano, "Photon upconversion based on sensitized triplet–triplet annihilation," *Coord. Chem. Rev.* **254**, 2560–2573 (2010).
3. J. Z. Zhao, S. M. Ji, and H. M. Guo, "Triplet–triplet annihilation based upconversion: from triplet sensitizers and triplet acceptors to upconversion quantum yields," *RSC Adv.* **1**, 937–950 (2011).
4. A. Monguzzi et al., "Low power, non-coherent sensitized photon up-conversion: modelling and perspectives," *Phys. Chem. Chem. Phys.* **14**, 4322–4332 (2012).
5. Y. C. Simon and C. Weder, "Low-power photon upconversion through triplet–triplet annihilation in polymers," *J. Mater. Chem.* **22**, 20817–20830 (2012).
6. J. H. Kim and J. H. Kim, "Encapsulated triplet–triplet annihilation-based upconversion in the aqueous phase for sub-band-gap semiconductor photocatalysis," *J. Am. Chem. Soc.* **134**, 17478–17481 (2012).
7. V. Gray et al., "Triplet–triplet annihilation photon-upconversion: towards solar energy applications," *Phys. Chem. Chem. Phys.* **16**, 10345–10352 (2014).
8. T. W. Schmidt and F. N. Castellano, "Photochemical upconversion: the primacy of kinetics," *J. Phys. Chem. Lett.* **5**, 4062–4072 (2014).
9. J. Zhou et al., "Upconversion luminescent materials: advances and applications," *Chem. Rev.* **115**, 395–465 (2015).
10. N. Yanai and N. Kimizuka, "Recent emergence of photon upconversion based on triplet energy migration in molecular assemblies," *Chem. Commun.* **53**, 655–655 (2017).
11. M. A. Filatov et al., "Reversible oxygen addition on a triplet sensitizer molecule: protection from excited state depopulation," *Phys. Chem. Chem. Phys.* **17**, 6501–6510 (2015).
12. Z. Y. Huang et al., "Hybrid molecule-nanocrystal photon upconversion across the visible and near-infrared," *Nano Lett.* **15**, 5552–5557 (2015).
13. K. Okumura et al., "Employing core-shell quantum dots as triplet sensitizers for photon upconversion," *Chem. Eur. J.* **22**, 7721–7726 (2016).
14. C. Mongin et al., "Direct observation of triplet energy transfer from semiconductor nanocrystals," *Science* **351**, 369–372 (2016).
15. Y. Sasaki et al., "Near infrared-to-blue photon upconversion by exploiting direct S-T absorption of a molecular sensitizer," *J. Mater. Chem. C* **5**, 5063–5067 (2017).

16. R. R. Islangulov et al., "Noncoherent low-power upconversion in solid polymer films," *J. Am. Chem. Soc.* **129**, 12652–12653 (2007).

17. J. H. Kim et al., "High efficiency low-power upconverting soft materials," *Chem. Mater.* **24**, 2250–2252 (2012).

18. F. Marsico et al., "Hyperbranched unsaturated polyphosphates as a protective matrix for long-term photon upconversion in air," *J. Am. Chem. Soc.* **136**, 11057–11064 (2014).

19. S. H. Lee et al., "Glassy poly(methacrylate)terpolymers with covalently attached emitters and sensitizers for low-power light upconversion," *J. Polym. Sci. A Polym. Chem.* **53**, 1629–1639 (2015).

20. A. Monguzzi et al., "Solid-state sensitized upconversion in polyacrylate elastomers," *J. Phys. Chem. C* **120**, 2609–2614 (2016).

21. R. Vadrucci, C. Weder, and Y. C. Simon, "Low-power photon upconversion in organic glasses," *J. Mater. Chem. C* **2**, 2837–2841 (2014).

22. P. F. Duan et al., "Photon upconversion in supramolecular gel matrixes: spontaneous accumulation of light-harvesting donor–acceptor arrays in nanofibers and acquired air stability," *J. Am. Chem. Soc.* **137**, 1887–1894 (2015).

23. T. Ogawa et al., "Highly efficient photon upconversion in self-assembled light-harvesting molecular systems," *Sci. Rep.* **5**, 10882 (2015).

24. P. F. Duan et al., "Aggregation-induced photon upconversion through control of the triplet energy landscapes of the solution and solid states," *Angew. Chem. Int. Ed.* **54**, 7544–7549 (2015).

25. T. C. Wu, D. N. Congreve, and M. A. Baldo, "Solid state photon upconversion utilizing thermally activated delayed fluorescence molecules as triplet sensitizer," *Appl. Phys. Lett.* **107**, 031103 (2015).

26. S. Hisamitsu, N. Yanai, and N. Kimizuka, "Photon-upconverting ionic liquids: effective triplet energy migration in contiguous ionic chromophore arrays," *Angew. Chem. Int. Ed.* **54**, 11550–11554 (2015).

27. J. S. Lissau et al., "Photon upconversion from chemically bound triplet sensitizers and emitters on mesoporous ZrO_2: implications for solar energy conversion," *J. Phys. Chem. C* **119**, 25792–25806 (2015).

28. M. Hosoyamada et al., "Molecularly dispersed donors in acceptor molecular crystals for photon upconversion under low excitation intensity," *Chem. Eur. J.* **22**, 2060–2067 (2016).

29. M. Oldenburg et al., "Photon upconversion at crystalline organic–organic heterojunctions," *Adv. Mater.* **28**, 8477–8482 (2016).

30. A. Monguzzi et al., "Unraveling triplet excitons photophysics in hyper-cross-linked polymeric nanoparticles: toward the next generation of solid-state upconverting materials," *J. Phys. Chem. Lett.* **7**, 2779–2785 (2016).

31. N. Kimizuka, N. Yanai, and M. Morikawa, "Photon upconversion and molecular solar energy storage by maximizing the potential of molecular self-assembly," *Langmuir* **32**, 12304–12322 (2016).

32. K. Kamada et al., "Efficient triplet–triplet annihilation upconversion in binary crystalline solids fabricated via solution casting and operated in air," *Mater. Horiz.* **4**, 83–87 (2017).

33. S. Baluschev et al., "Two pathways for photon upconversion in model organic compound systems," *J. Appl. Phys.* **101**, 023101 (2007).

34. H. Goudarzi and P. E. Keivanidis, "Triplet–triplet annihilation-induced up-converted delayed luminescence in solid-state organic composites: monitoring low energy photon up-conversion at low temperatures," *J. Phys. Chem. C* **118**, 14256–14265 (2014).

35. Q. H. Cui, Y. S. Zhao, and J. N. Yao, "Controlled synthesis of organic nanophotonic materials with specific structures and compositions," *Adv. Mater.* **26**, 6852–6870 (2014).

36. B. Li et al., "Nonequilibrium self-assembly of π-conjugated oligopeptides in solution," *ACS Appl. Mater. Interfaces* **9**, 3977–3984 (2017).

37. H. A. M. Ardona et al., "Kinetically controlled coassembly of multichromophoric peptide hydrogelators and the impacts on energy transport," *J. Am. Chem. Soc.* **139**, 8685–8692 (2017).

38. X. J. Zhang et al., "Single-crystal 9,10-diphenylanthracene nanoribbons and nanorods," *Chem. Mater.* **20**, 6945–6950 (2008).

39. B. Yang et al., "Shape-controlled micro/nanostructures of 9,10-diphenylanthracene (DPA) and their application in light-emitting devices," *J. Phys. Chem. C* **115**, 7924–7927 (2011).

40. C. Zhang et al., "Self-modulated white light outcoupling in doped organic nanowire waveguides via the fluctuations of singlet and triplet excitons during propagation," *Adv. Mater.* **23**, 1380–1384 (2011).

41. M. Campione et al., "Control of $\pi - \pi$ interactions in epitaxial films of platinum(II) octaethyl porphyrin," *Chem. Mater.* **23**, 832–840 (2011).

42. A. Monguzzi et al., "Upconversion-induced fluorescence in multicomponent systems: steady-state excitation power threshold," *Phys. Rev. B* **78**, 195112 (2008).

43. Y. Y. Cheng et al., "On the efficiency limit of triplet–triplet annihilation for photochemical upconversion," *Phys. Chem. Chem. Phys.* **12**, 66–71 (2010).

44. A. Haefele et al., "Getting to the (square) root of the problem: how to make noncoherent pumped upconversion linear," *J. Phys. Chem. Lett.* **3**, 299–303 (2012).

45. N. Yanai et al., "Increased vis-to-UV upconversion performance by energy level matching between a TADF donor and high triplet energy acceptors," *J. Mater. Chem. C* **4**, 6447–6451 (2016).

46. V. Gray et al., "Loss channels in triplet–triplet annihilation photon upconversion: importance of annihilator singlet and triplet surface shapes," *Phys. Chem. Chem. Phys.* **19**, 10931–10939 (2017).

47. S. Amemori et al., "Near-infrared-to-visible photon upconversion sensitized by a metal complex with spin-forbidden yet strong S_0-T_1 absorption," *J. Am. Chem. Soc.* **138**, 8702–8705 (2016).

48. M. F. Wu et al., "Solid-state infrared-to-visible upconversion sensitized by colloidal nanocrystals," *Nat. Photonics* **10**, 31–34 (2016).

Taku Ogawa received his MS degree in engineering from Kyushu University in 2015. He is currently a PhD candidate under the supervision of Prof. N. Kimizuka and Dr. N. Yanai in the Department of Chemistry and Biochemistry. His current research focuses on triplet energy dynamics in self-assembled materials.

Nobuhiro Yanai received his PhD from Kyoto University in 2011 with Prof. Susumu Kitagawa and Dr. Takashi Uemura on polymer properties in MOFs. He was a postdoctoral researcher with Prof. Steve Granick at the University of Illinois at Urbana–Champaign, working on self-assembly of MOF colloids. In 2012, he became an assistant professor at Kyushu University, where he has been an associate professor since 2015. His current research interests are in materials chemistry for photon upconversion.

Hironori Kouno received his MS degree in engineering from Kyushu University in 2017. He is currently a PhD candidate under the supervision of Prof. N. Kimizuka and Dr. N. Yanai in the Department of Chemistry and Biochemistry. His current research focuses on establishment of aqueous photon upconversion molecular system. His research interests also include development of functional materials for energy-related and biological applications.

Nobuo Kimizuka received his PhD from Kyushu University in 1990 with Prof. Toyoki Kunitake on the excitonic chromophore interactions in molecular membranes. After working as a post-doctoral researcher with Prof. Helmut Ringsdorf at Mainz University, he was promoted to an associate professor in 1992 and a full professor in 2000. His work encompasses the synthesis and functions of molecular self-assemblies and nanomaterials with recent focus on photon energy conversion in organized molecular systems.